The Effect of Irradiation on Structural and Optical Characteristics of Indium Oxide Thin Films

Sanaa Rasool Salim

Department of Physics, College of Science, Al Mustansiriyah University, Baghdad, Iraq

Abstract: *In_2O_3 film was obtained by thermal oxidation of indium film under vacuum pressure down 10^{-4} Torr using tube quartz. The temperature-time oxidation cycle is shown in Figure (1) the condition used in this study to prepare In_2O_3 was 400°C/45min. The X-ray diffraction (XRD) spectrum of the film recorded with X-ray diffractometer operates with 1.5417A monochromatized CuKα radiation with Ni filter. The film transmittance was measured in the range (300-900) nm using Shimadzu spectrophotometer.*

Keyword: Indium oxide films; Optical band gap; Beta-ray; thermal oxidation

1. Introduction

Indium oxide (In_2O_3) is n-type highly degenerate, wide band gap semiconductor which exhibits high electrical conductivity and high optical transparency in the visible light region [1]. These unique properties are extensively useful as transparent conductors in optoelectronic devices such as transparent electrodes for flat panel displays [2], selective transparent coatings for solar energy heat mirrors [3] and window layers in heterojunction solar cells [4, 5]. A wide range of thin film deposition techniques such as vacuum evaporation [6–8], thermal oxidation of indium films [9], pulsed laser deposition [10–12], atomic layer epitaxial growth [13], spin coating [14], sol-gel process [15], ion assisted deposition [16], and dc and rf sputtering [17–21] were employed for preparation of indium oxide films. In_2O_3 thin films have a good adherence to the substrate surface and high chemical inertness [22]. In general, undoped binary oxide films are insulators in their stoichiometric form. On the other hand, this property can be changed by suitable doping and controlling the concentration of oxygen vacancies. In_2O_3 can appear in two stable modifications as body-centered (bcc) cubic (a = 10.118°A) and rhombohedral (rh) (a = 5.478°A and c = 14.51°A) (crystallographic data are taken from [23]). They can be stabilized by choosing appropriate deposition conditions or synthesis methods [24, 25]. The rhombohedral phase has been rarely produced and it exhibits better physical properties than the cubic one. The difference seems to be the results packing of the anion layers in the rhombohedral In_2O_3 [26].

The beta sources were Sr^{90}/ Y^{90} obtained from AMERSHAM – UK. It is apoint sources of 0.1 cm diameter glass bead sealed in a welded stainless steel case, the activity at the time of the experiment was determined to be 5 mci. Sr^{90}/ Y^{90} is apure β – emitter , has tow beta groups , Sr^{90} decays into Y^{90} with the emission of beta particles of maximum energy 0.546 Mev and half – life of 28.82 years. Y^{90} decays to Sr^{90} with half – life of 64 hr with the emission of beta particales of maximum energy 2.274 Mev to the ground state with 99.98 % probability; and 0.02 % to the meta – state of Sr^{90} at 1.734 Mev with the emission of 1.734 Mev gama – rays. The intensity of the 1.734 Mev is very weak, therefore it is hardly detectable. Energy spectrum at the region less than 540Mev is amixture of the tow isotopes Sr^{90} and Y^{90} [27].

In the present work, the main characteristic of In_2O_3 thin film has been investigated and analyzed before and after irradiation of β-rays at room temperature with different irradiation time.

2. Experiment Work

Thermal evaporation system type Edwards (E-306A) high vacuum coating unit [28] was used to evaporate high purity indium (99.9 %) having thickness around (100, 150, 200) nm on glass slides each of 3×2.5 cm^2 area under low pressure (~ 10^{-6} torr). In_2O_3 film was obtained by thermal oxidation of indium film under vacuum pressure down 10^{-4} Torr using tube quartz. The temperature-time oxidation cycle is shown in Figure (1) the condition used in this study to prepare In_2O_3 was 400°C/45min. Test glass slides, cleaned by alcohol with ultrasonic waves in order to remove the impurities and residuals from their surfaces. The X-ray diffraction (XRD) spectrum of the film recorded with X-ray diffractometer operates with 1.5417A monochromatized CuKα radiation with Ni filter. The film transmittance was measured in the range (300-900) nm using Shimadzu spectrophotometer.

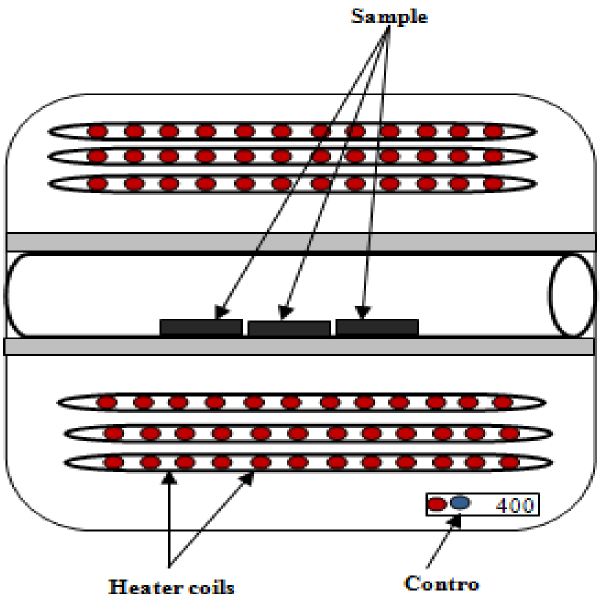

Figure 1: Thermal oxidation system

3. Results and Discussion

3.1. Structural properties of In_2O_3 films

The typical XRD diffractograms taken from the indium oxide layer after prepared at 400 ◦C for 45 min is shown in figure (2). The XRD patterns revealed a clear polycrystalline structure. The diffraction pat3terns consist of diffraction peaks related to the (bcc) structure of In_2O_3 and corresponding to (222), (400) lattice planes correlating with the results obtained in [5]. The strongest diffraction peak is the peak related to the (222) lattice plane indicating corresponding preferential orientation along this direction.

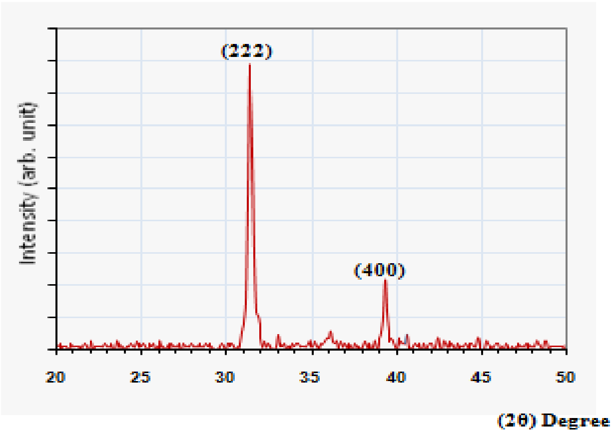

Figure 2: XRD of In_2O_3 thin film

The films of In_2O_3, thickness 100 nm, 150 nm and 200 nm are prepared onto glass substrate at a pressure of about 10^{-6} Torr for studying the optical properties of In_2O_3 films. The measurements for In_2O_3 film before and after irradiation of β-rays at room temperature in the wavelength of 300 to 900 nm. The variation of transmittance and reflectance with wavelength for In_2O_3 films before and after irradiation of β-rays at different iradation times are shown in figure (3) (a, b, c, d) and (4) (a, b, c, d) respectively.

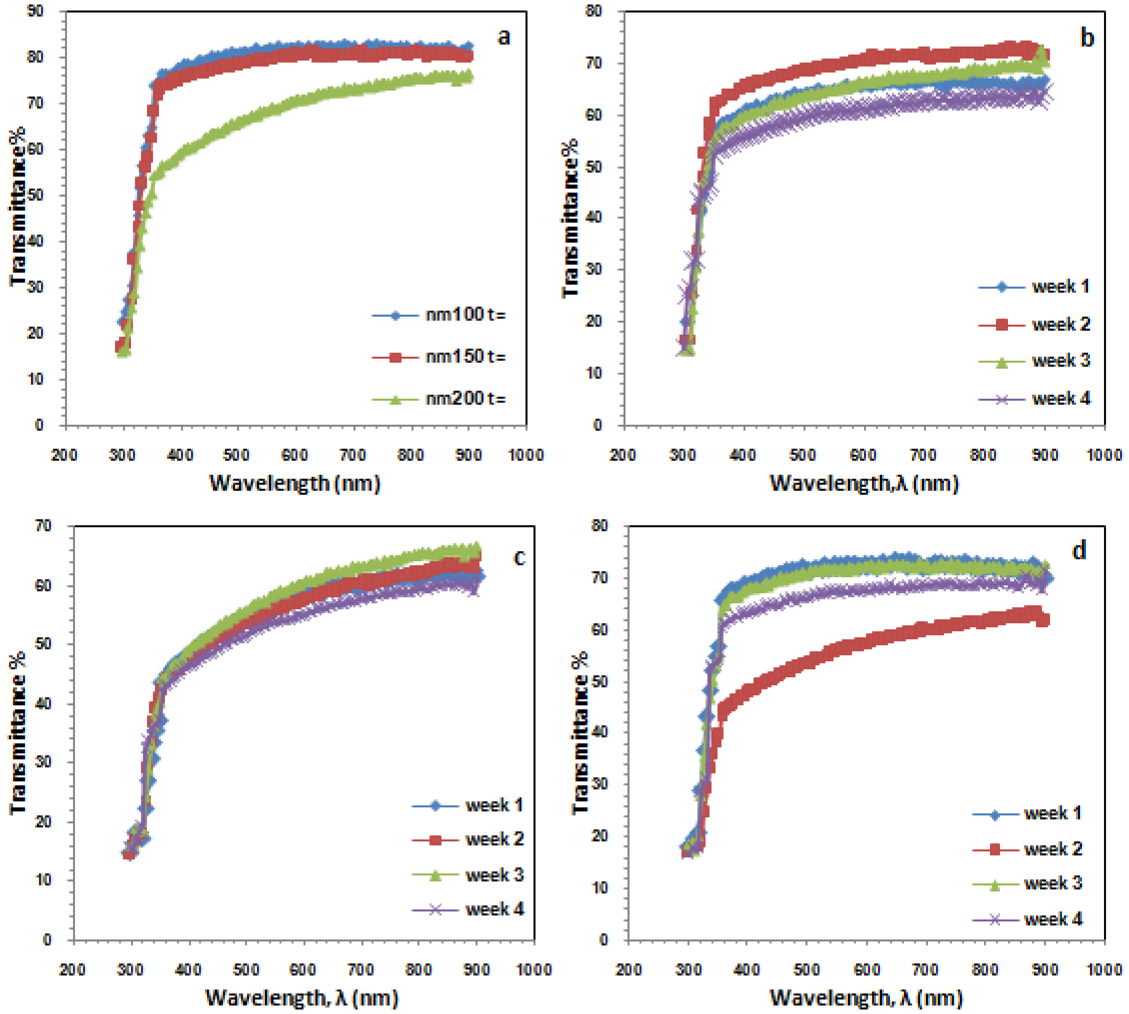

Figure 3: Variation of transmittance with wave length for In_2O_3 films of different irradiation times (a) before (b) t= 100 nm, (c) t= 150 nm and (d) t= 200 nm.

It is seen from the graph of figure (3) that the value of transmittance is low in the ultraviolet region. In the visible region, the transmittance is high whereas it decrease in the near-infrared region. It is also observed from the graph of figure (3) that the value of reflectance is low in the ultraviolet region and increase in the visible region. The improved transmission in the short wavelength region and the peak transmission was in excess of 82% at thicknesses of 100 nm is attributed to the well adherent and crystallized nature of the film throughout the coated area, which is obtained due to uniform oxidation and improvement in lattice arrangement. Also the transmittance decrease but the reflectance increase with the increase of films thickness. The reduced %T behavior at higher thickness may be due to impaired crystallinity of the films as evident from the XRD results figure (2), which showed peaks with reduced intensity. After irradiation, the transmittance decrease.

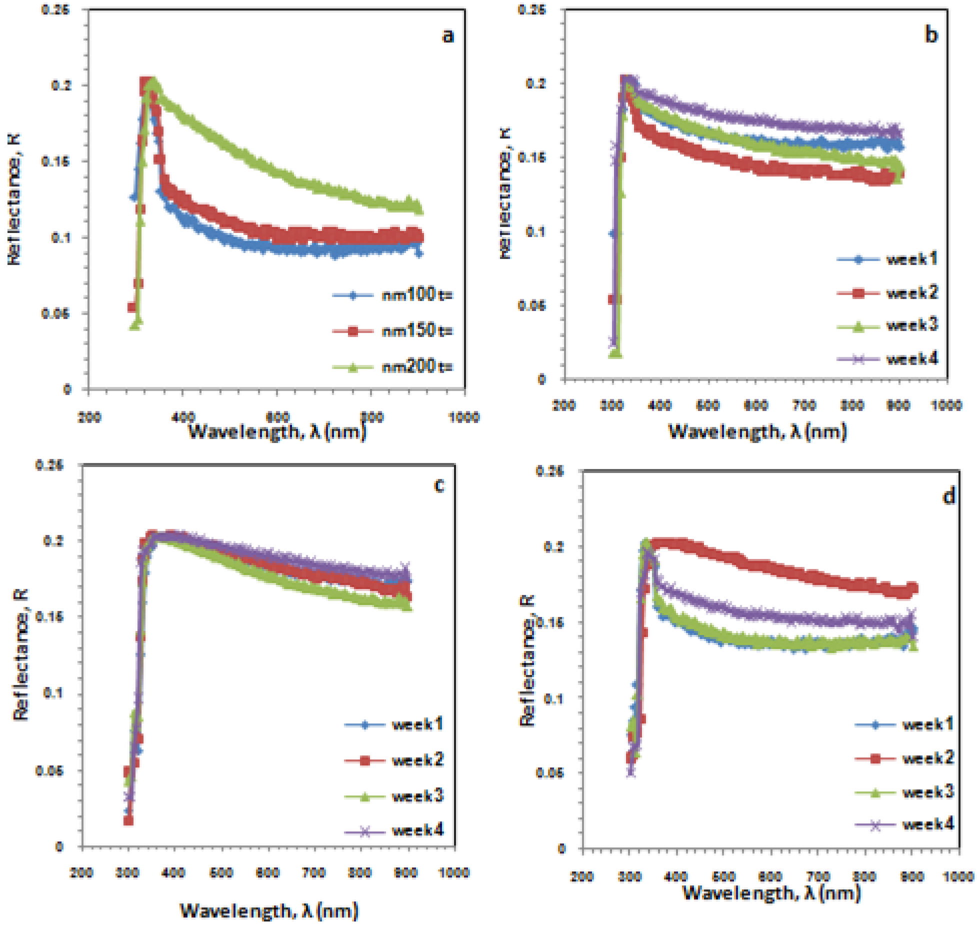

Figure 4: Variation of reflectance with wave length for In_2O_3 films of different irradiation times (a) before (b) t= 100 nm, (c) t= 150 nm and (d) t= 200 nm

The variation of absorbance with wavelength for In_2O_3 films before and after irradiation of β-rays at different iradation times are shown in figure (5). The absorbance is very high in the ultraviolet region whereas its value decreases in the visible and near-infrared region as shown in figure (4). The absorbance increase after irradiation.

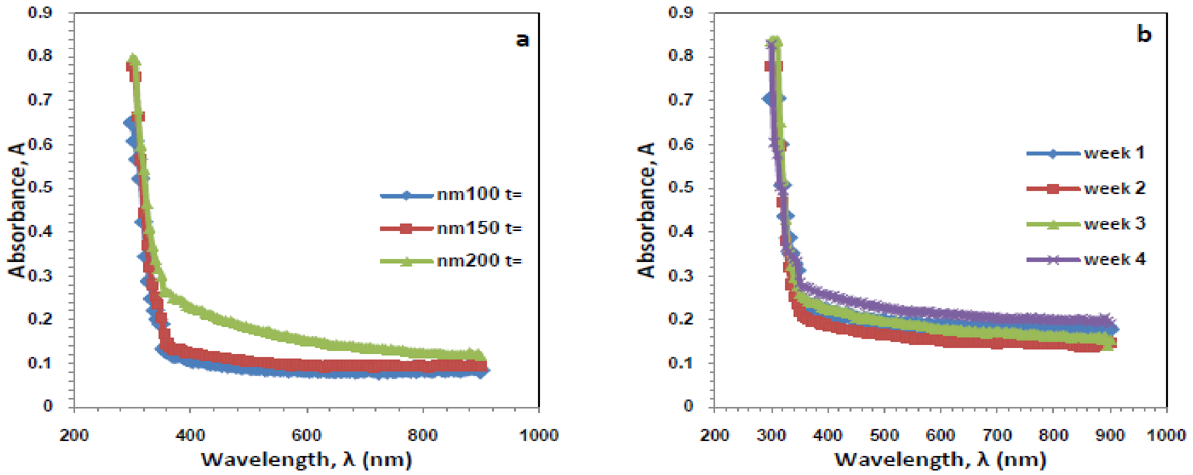

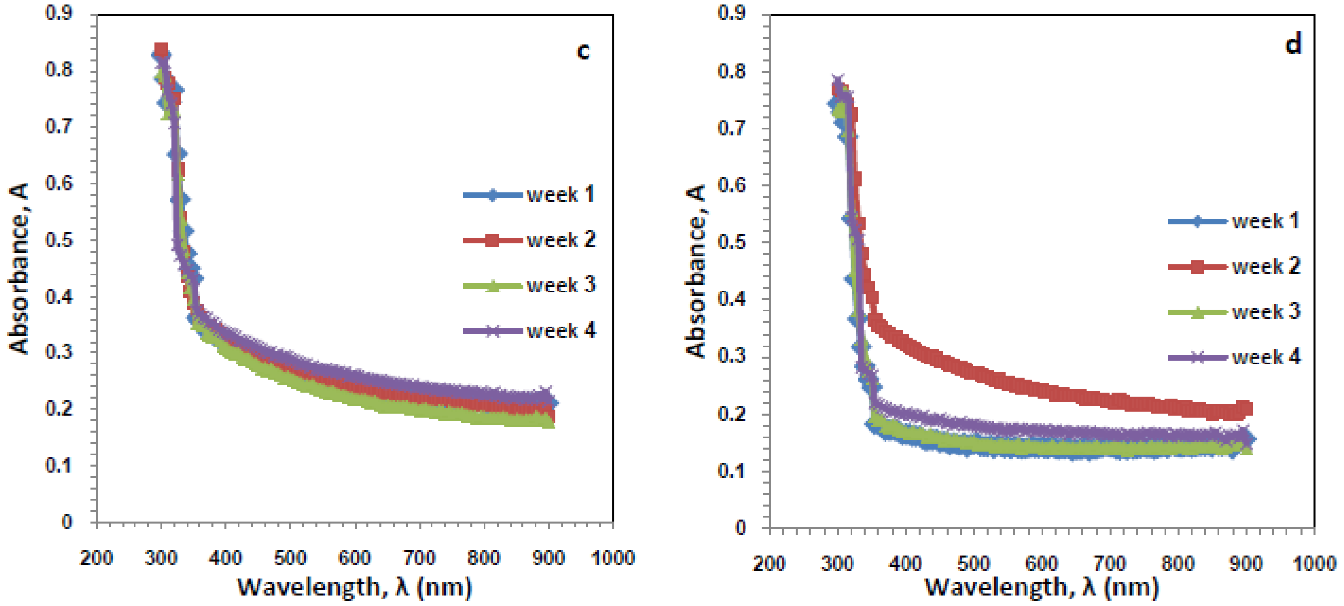

Figure 5: Variation of absorbance with wave length for In_2O_3 films of different irradiation times (a) before (b) t= 100 nm, (c) t= 150 nm and (d) t= 200 nm

Analysis of optical absorption spectra is one of the most productive tools for understanding and developing the band structure and energy gap. The optical band gap of polycrystalline In_2O_3 films was calculated from the optical absorption and transmission studies. The optical absorption A is related to the band gap of a semiconductor film, which satisfies the equation [1]:

$$\alpha h\gamma = A(h\gamma - E_g)^n \text{……………..} \quad (1)$$

Where hν is the photon energy, α the absorption coefficient, E_g the band gap, A is the constant, (n) =1/2 for direct band gap material and (n) =2 for indirect band gap. Plots of $(\alpha h\nu)^2$ vs. (hν) for direct allowed transition of different films thickness is shown in figure (6) before and after irradiation of beta-ray. The value of energy gap is evaluated from the graph of figure (6) and is found to be ~3.7 eV. This suggests that In_2O_3 is a direct band gap material. The band gap increase after irradiation.

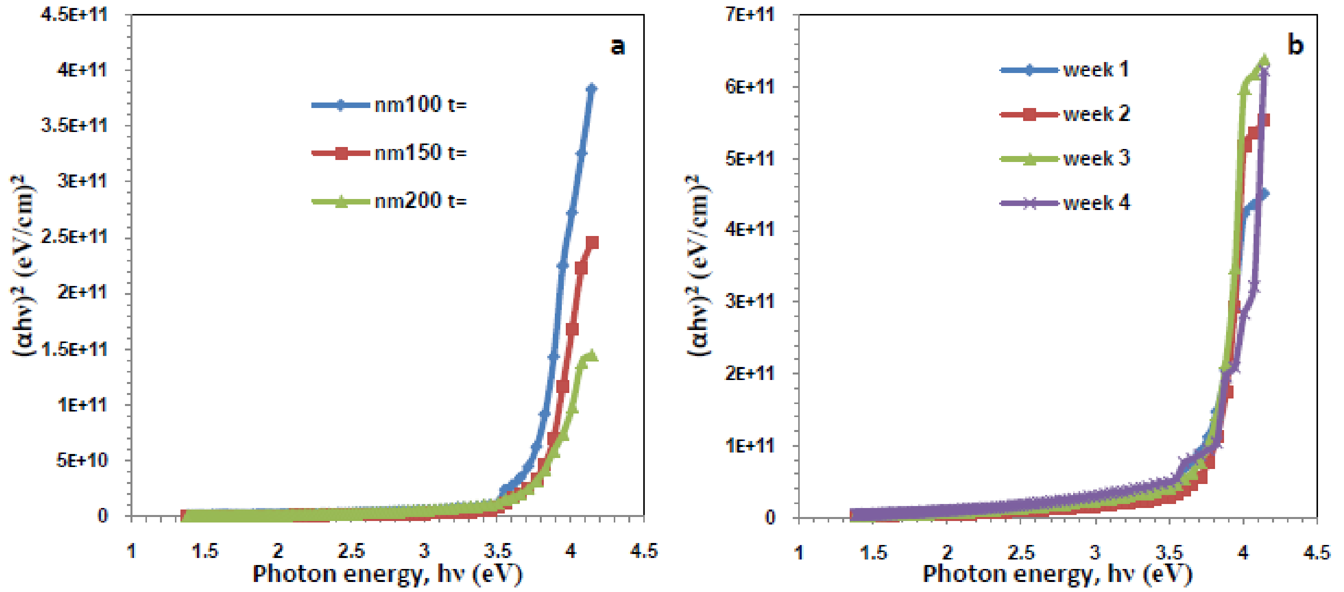

Figure 6: Variation of $(\alpha h\nu)^2$ with (hν) for In_2O_3 films of different irradiation times (a) before (b) t= 100 nm, (c) t= 150 nm and (d) t= 200 nm

The optical absorption coefficient (α) is related to the transmittance T of a sample with thickness t through the relation [7]:

$$\alpha = \frac{2.303}{t} \log\left(\frac{1}{T}\right) \text{………………..} \quad (2)$$

Where t is the film thickness

Figure (7) shows the optical absorption spectra [(plots of α^2 versus photon energy hν (wavelength range 300-900 nm)] obtained at room temperature of as-grown In_2O_3 films of different thickness. From the figure the absorption coefficient (α) increases with increasing photon energy for investigated thin films. We can evidently see that absorption coefficient having values ($\alpha > 10^4 cm^{-1}$) which leads to increase the probability of occurrence direct transition. It can be seen that the plot is linear in the region of strong absorption near the fundamental absorption edge. Thus, the absorption takes place through direct transition.

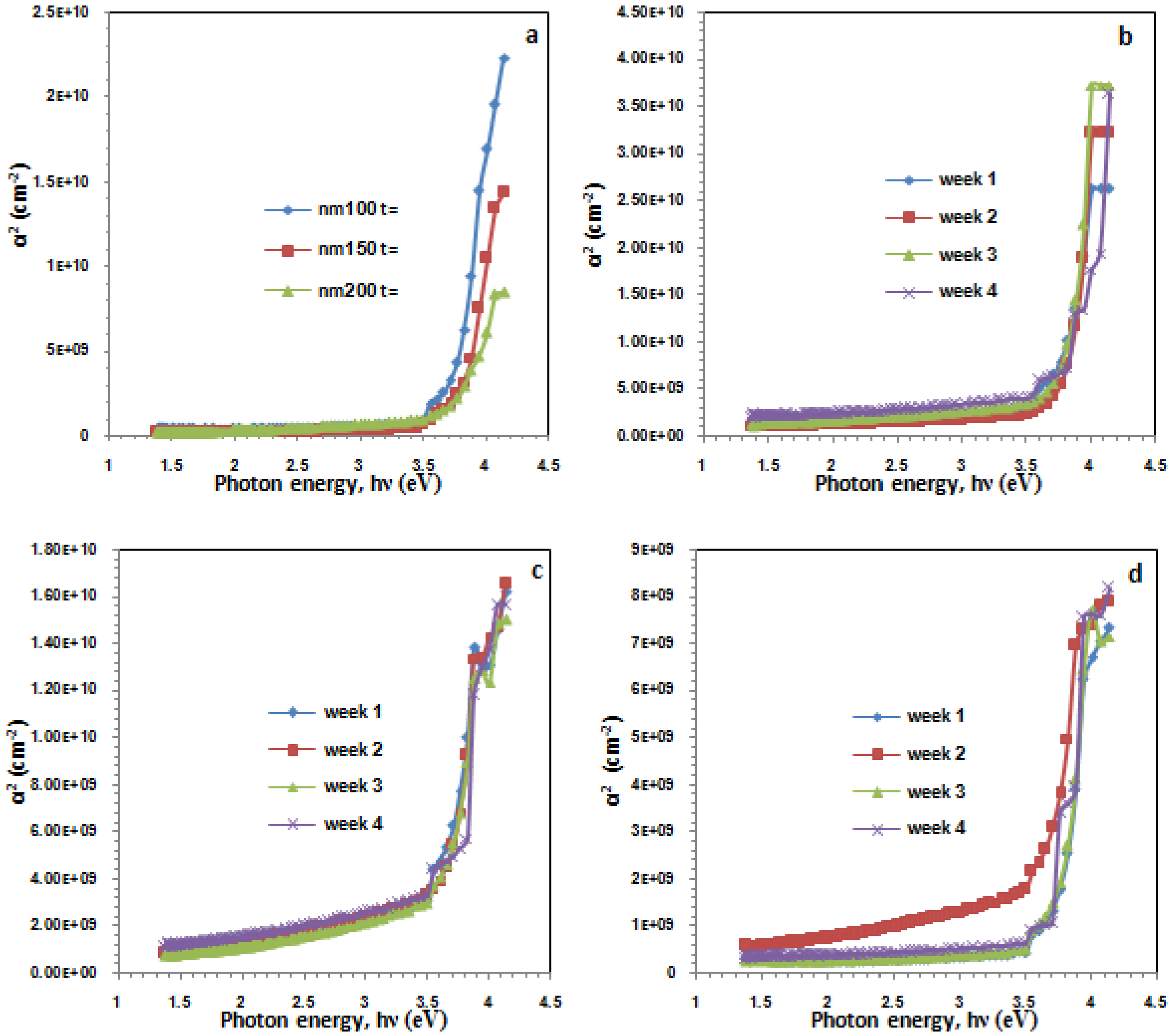

Figure 7: Variation of $(\alpha)^2$ with (hν) for In_2O_3 films of different irradiation times (a) before (b) t= 100 nm, (c) t= 150 nm and (d) t= 200 nm

The width of localized states is determined by using the following equation:

$$\ln\alpha = \ln\alpha_o + \frac{h\nu}{E_t} \ldots\ldots\ldots\ldots\ldots..(3)$$

The width of localized states is determined by plotting (lnα) versus photon energy (hν) then from inverse of the slope of the straight line of the curve we found the width of the localized states. Figure (8) show the variation of (lnα) with photon energy(hν) before and after irradiation of beta-ray for In_2O_3 thin films respectively.

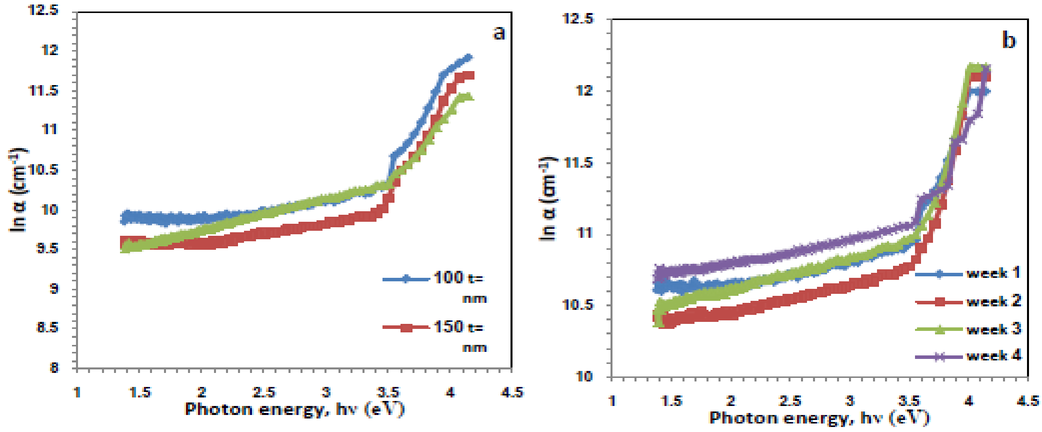

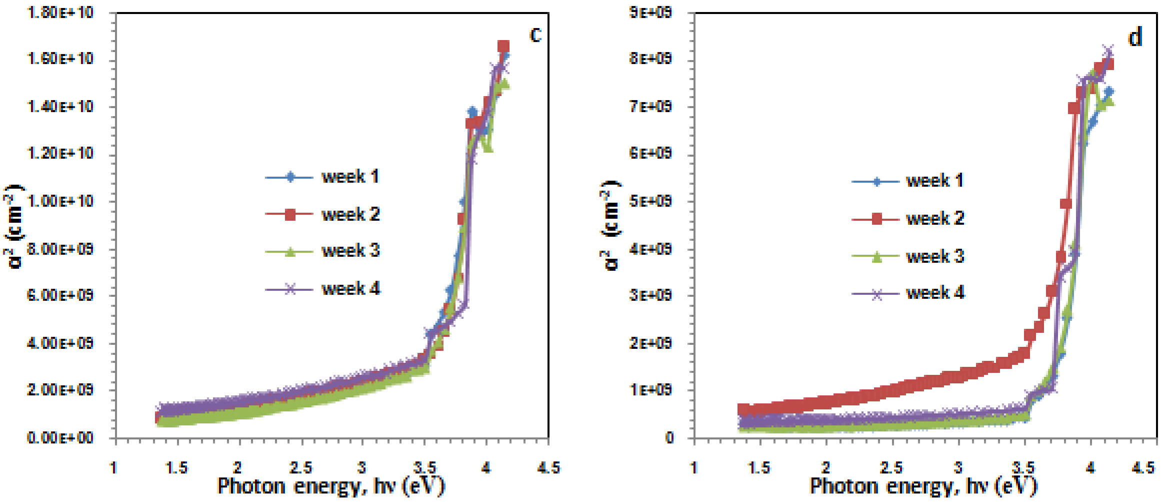

Figure 8: Variation of (lnα) with (hν) for In_2O_3 films of different irradiation times (a) before (b) t= 100 nm, (c) t= 150 nm and (d) t= 200 nm

The electromagnetic will have its amplitude reduced by a factor 'e' after traversing a thickness (called the skin depth) ξ such that:

$$\xi = \lambda / 2\pi k \ldots\ldots\ldots\ldots\ldots\ldots\ldots\ldots \text{(4)}$$

This may be the order of 100 to several thousand angstroms, depending on the material [13]. The skin depth calculated using the relation (4), figure (9) shows the variation of skin depth as a function of wavelength of the In_2O_3 thin film. It was mentioned that the depth will be increased with increasing the wavelength. The skin depth is transmission related, from this figure one can conclude:

- At short wavelengths close to the ($\lambda_{\text{cut-off}}$) , the probability of absorption highly increase and the amplitude of the incident photons will be reduced by a factor 'e' through the short distance within the film thickness , then the skin depth was decreased .
- At wavelengths greater than the ($\lambda_{\text{cut-off}}$) within the visible region, the absorption effect vanishes and the reduction in amplitude occurs after passing a larger distance, then the skin depth will increase.
- At IR region, the scattering (or reflection) clearly appeared, this may be cause re-decrease in skin depth.

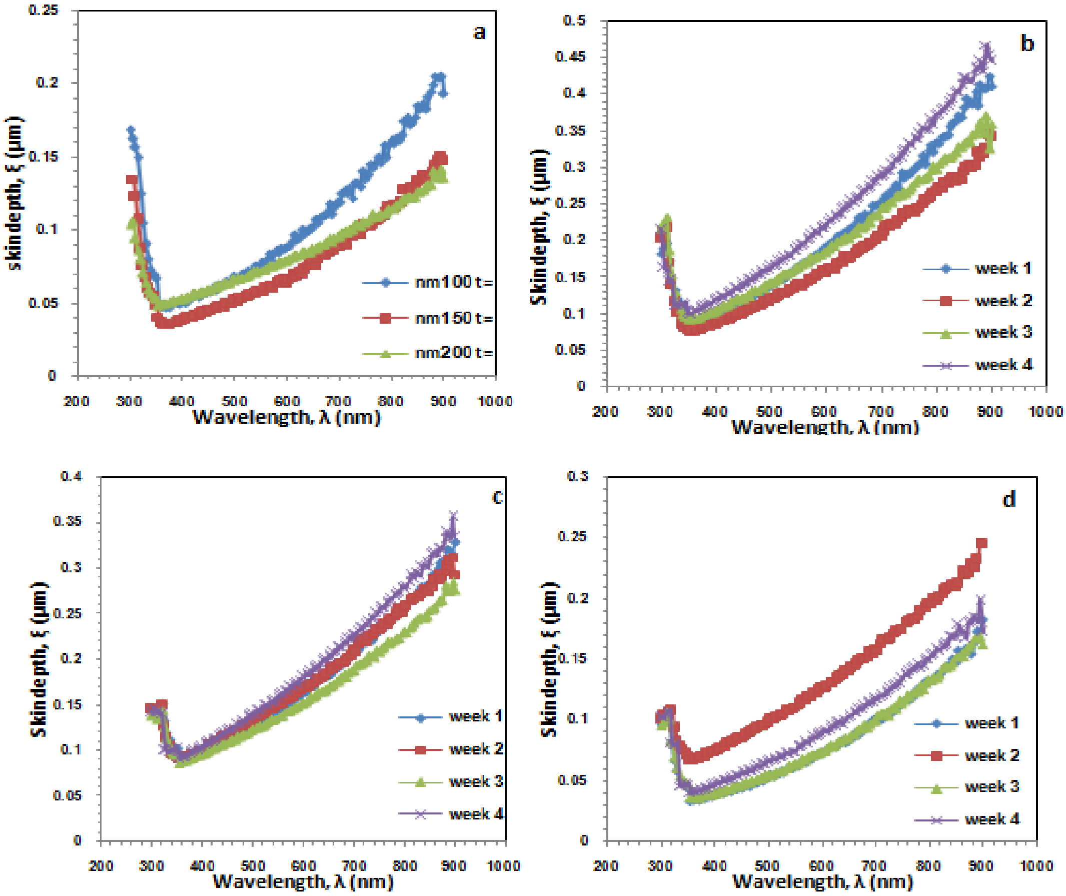

Figure 9: Variation of skin depth with wavelength for In_2O_3 films of different irradiation times (a) before (b) t= 100 nm, (c) t= 150 nm and (d) t= 200 nm

Cut-off wavelength refer to the absorption edge , $\lambda_{\text{cut-off}}$ of In_2O_3 thin films can determine from absorption coefficient by plotting α vs. λ , the extrapolating line across λ axis indicates the magnitude of $\lambda_{\text{cut-off}}$. Also it can be calculated from the energy gap as in relation:

$$\lambda_{\text{cut-off}} = 1.24/E_g \ldots\ldots\ldots\ldots\ldots\ldots\ldots (5)$$

From the absorption coefficient and energy gap results, and returning to the figure (7) one can find the cut-off wavelength by extrapolating line at (α = o). Figure (10) (a, b) shows the plot of cut-off wavelength vs. thickness and [-----]. It is a clear that experimental values have the same variation up to (t =150 nm) and then the divergence increase for higher values. The shifting to the higher values in the experimental cut-off wavelength could be attributed to the increase of contaminating impurity concentration with increasing film thickness, especially higher than (t =150 nm).

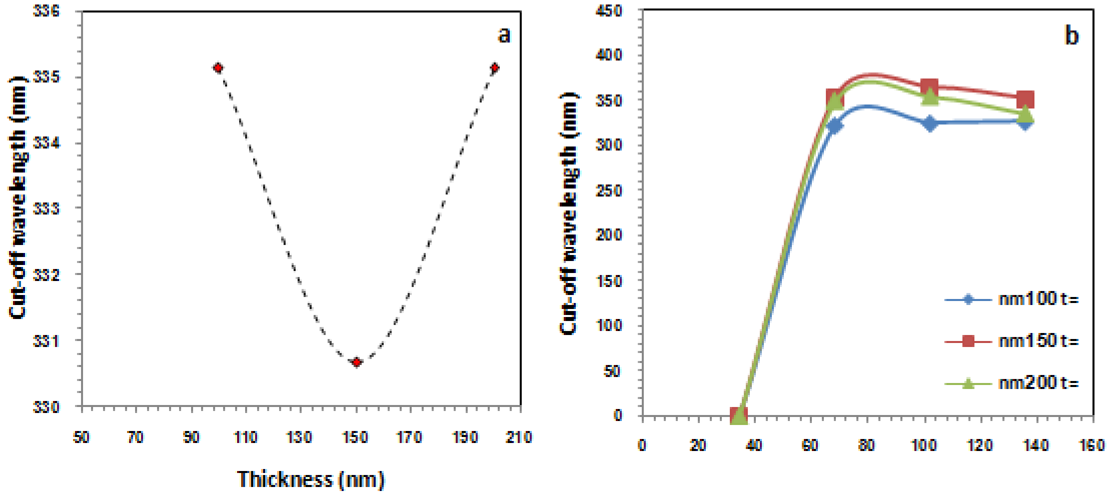

Figure 10: Variation of cut-off wavelength with (a) thickness (b) for In_2O_3

The extinction coefficient k_o was calculated by the following equation [21]:

$$k_0 = \frac{\alpha\lambda}{4\pi} \ldots\ldots\ldots\ldots\ldots\ldots\ldots\ldots\ldots\ldots\ldots\ldots\ldots (6)$$

Where α is the absorption coefficient of the film and λ is the wavelength of electromagnetic wave. The relation of k_o against wavelength are displayed in figure (11). It is also observed from the graph of figure (11) that the value of extinction coefficient is high in the ultraviolet region and low in the near-infrared region and extinction coefficient depends on the absorption coefficient (α), which is presumably increased with increasing the tail states width.

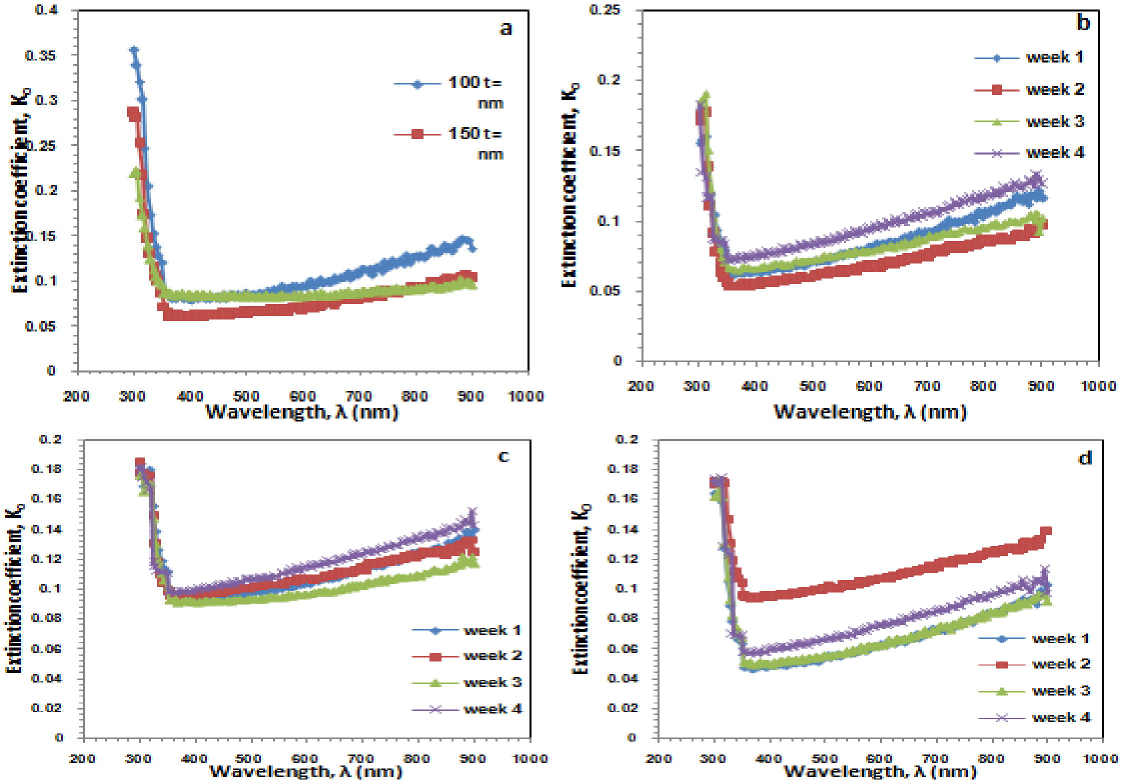

Figure 11: Variation of extinction coefficient with wave length for In_2O_3 films of different irradiation times (a) before (b) t= 100 nm, (c) t= 150 nm and (d) t= 200 nm

The equation used to calculate the refractive index n_o is [25]:

$$n_\circ = \left[\left(\frac{1+R}{1\text{-}R}\right)^2 - \left(k_\circ^{\,2}+1\right)\right]^{1/2} + \frac{1+R}{1-R} \ldots\ldots\ldots\ldots\ldots (7)$$

Figure (12) show the variation of refractive index with wavelength for In_2O_3 films before and after irradiation of β-rays at different iradation times. The values of refractive index low in the ultraviolet region and gradually increase with wavelength from the visible.

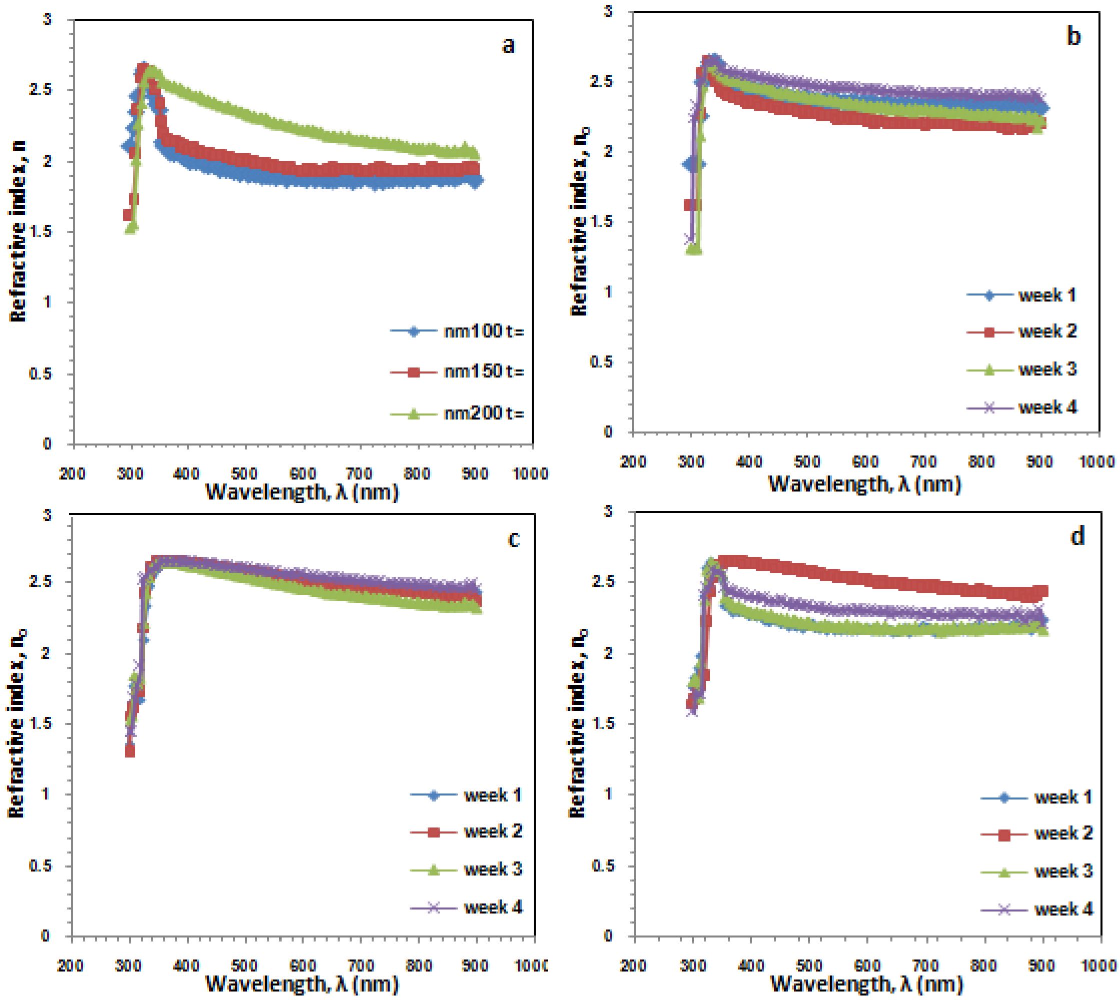

Figure 12: Variation of refractive index with wave length for In2O3 films of different irradiation times (a) before (b) t= 100 nm, (c) t= 150 nm and (d) t= 200 nm.

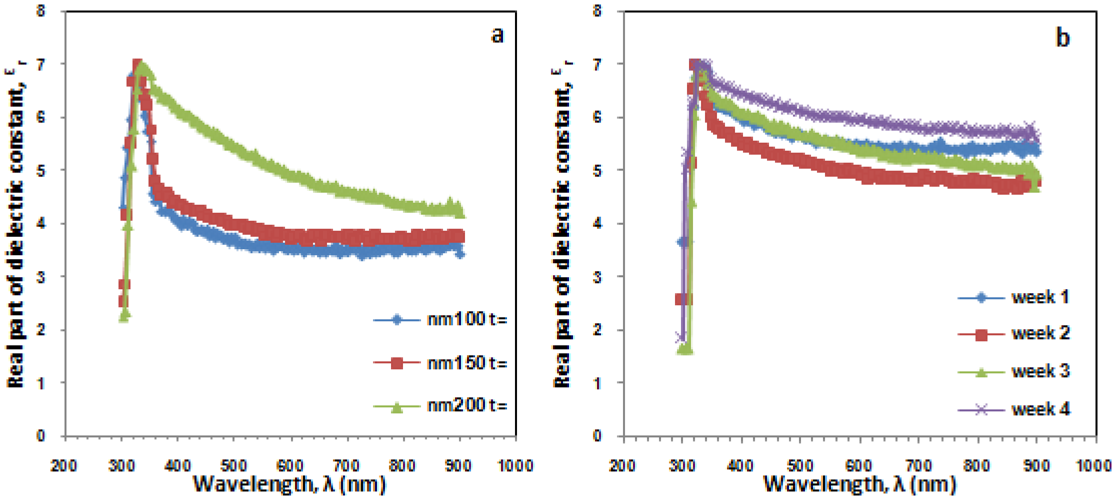

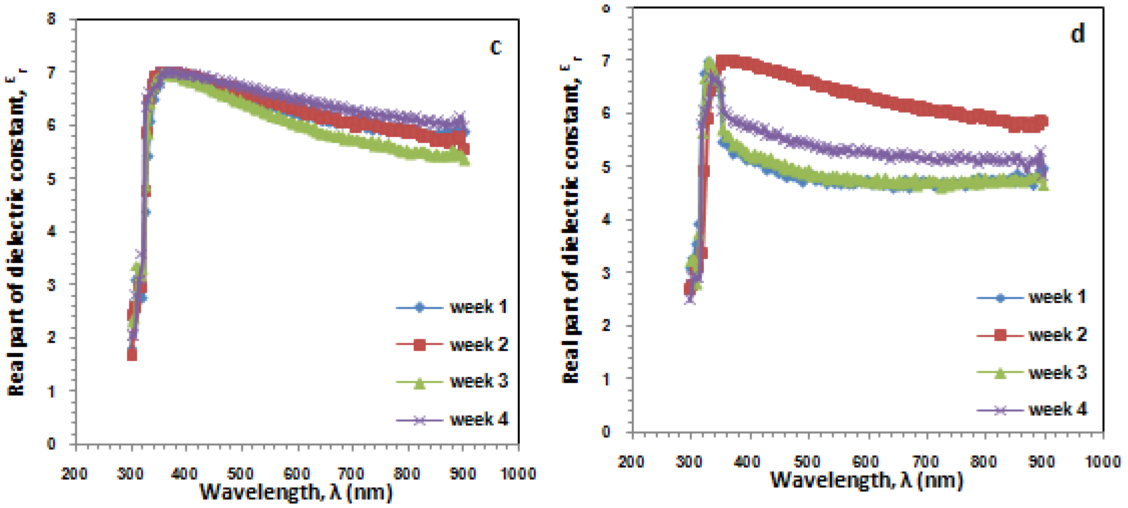

Figure 13: Variation of real dielctric constant with wave length for In_2O_3 films of different irradiation times (a) before (b) t= 100 nm, (c) t= 150 nm and (d) t= 200 nm

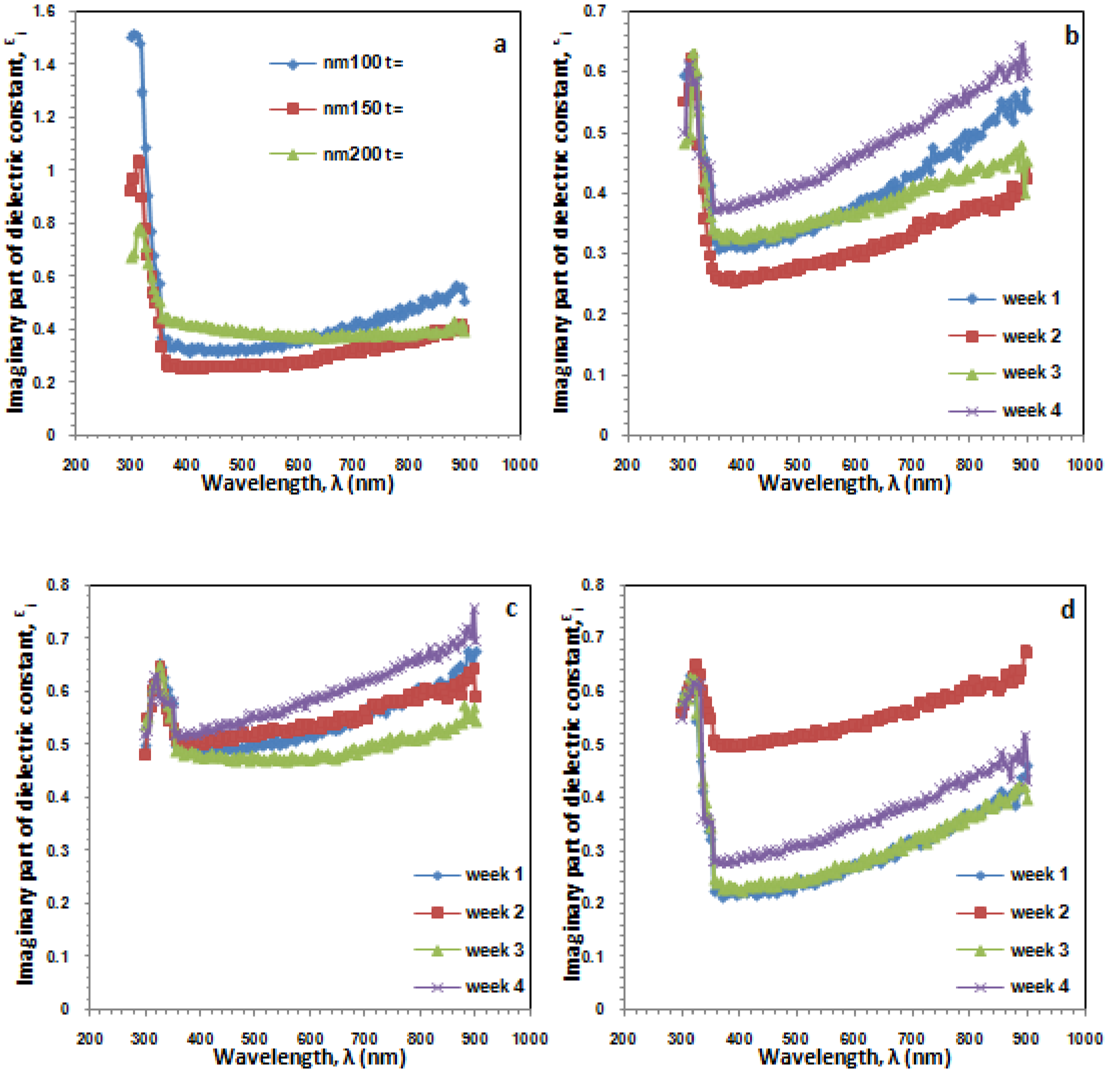

Figure 14: Variation of imaginary dielctric constant with wave length for In_2O_3 films of different irradiation times (a) before (b) t= 100 nm, (c) t= 150 nm and (d) t= 200 nm

The complex refractive index is one of the most important optical constants. The relation of the complex refractive index of In_2O_3 with the incident photon energy was determined as shown in figure (15). The observed uniformity in the behavior of the complex refractive index is an indication to the high uniformity of the optical properties of this material as a function of the incident photon energy.

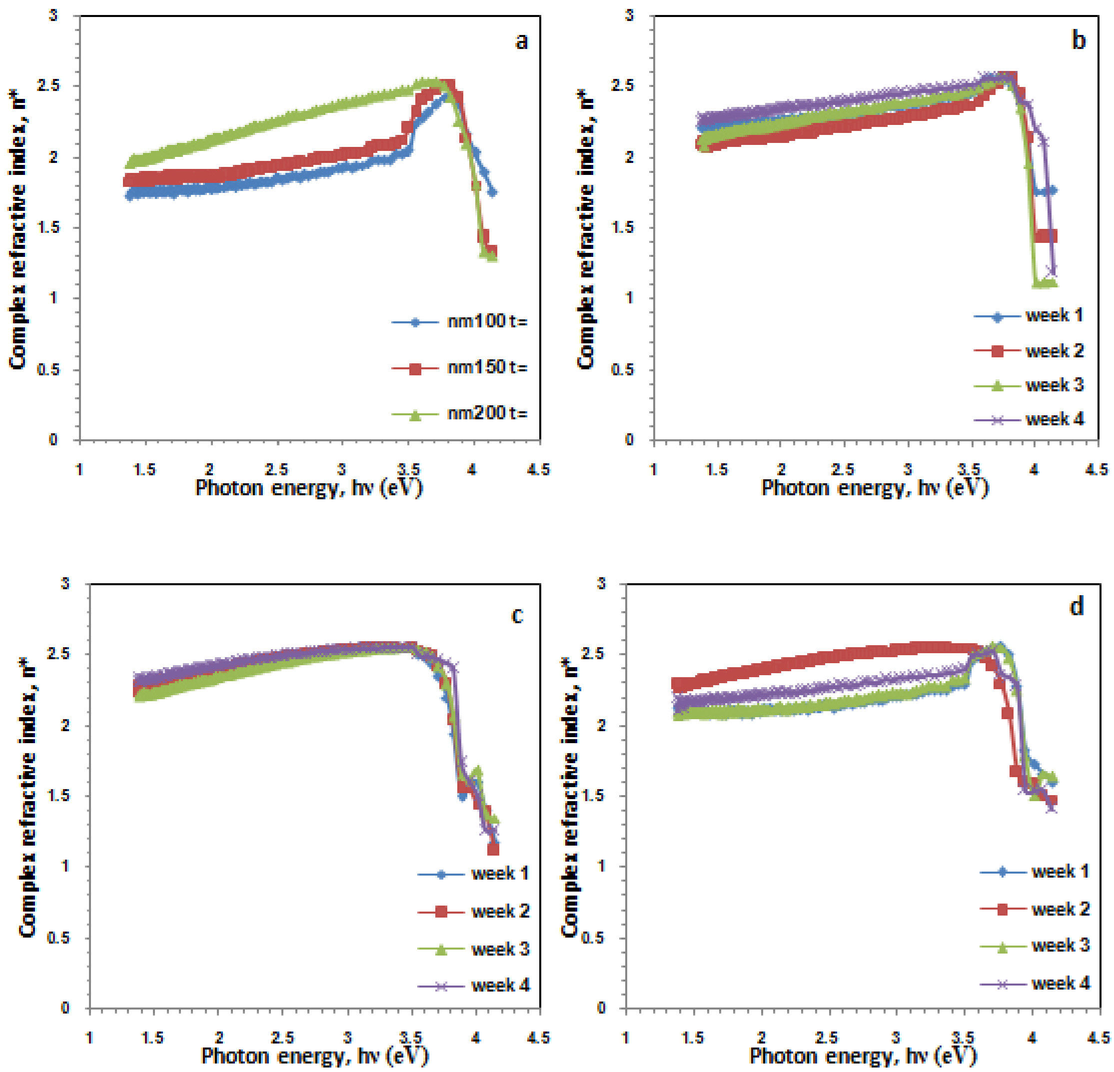

Figure 15: Variation of complex refractive index with photon energy for In_2O_3 films of different irradiation times (a) before (b) t= 100 nm, (c) t= 150 nm and (d) t= 200 nm

4. Conclusions

In_2O_3 film was obtained by thermal oxidation of indium film under vacuum pressure down 10^{-4} Torr using tube quartz. The condition used in this study to prepare In_2O_3 was 400°C/45min. The X-ray diffraction (XRD) spectrum of the film recorded with X-ray diffractometer operates with 1.5417A monochromatized CuKα radiation with Ni filter. The film transmittance was measured in the range (300-900) nm using Shimadzu spectrophotometer.

References

[1] J. I. Jeong, J. H. Moon, J. H. Hong, J. S. Kang, Y. Fukuda, Y. P. Lee, J. Vac. Sci. Technol. **A14**, 293 (1996).
[2] H. J. Glasser, Glass Technol. Ber. **50**, 1912 (1977).
[3] J. C. C. Fan, F. J. Bachner, J. Electrochem. Soc. **12**, 1719 (1975).
[4] T. Nagamoto, O. Omoto, Jpn. J. Appl. Phys. **14**, 915 (1976).
[5] T. A. Gessert, X. Li, M. W.Wanless, A. J. Nelson, T. J. Couts, J. Vac. Sci. Technol.,**A6**, 1912 (1990).
[6] S. Naseem, M. Iqbal, K. Hussain, Solar EnergyMater. Solar Cells **31**, 155 (1993).
[7] E. Baba Ali, H. El Maliki, J. C. Bernede, M. Sahnoun, A. Khelil, O. Saadene, Mater. Chem. Phys. **73,** 78 (2002).
[8] S. Nakamura,, Jpn. J. Appl. Phys., **30,** L 2062 (1991).
[9] V. Damodara Das, S. Kirupavathy, L. Damodara, N. Lakshminarayana, J. Appl. Phys.**79,** 8521 (1996).
[10] Y. Yamada, N. Suzuki, T. Makino, T. Yoshida, J. Vac. Sci. Technol. **A18,** 83 (2000).
[11] F. O. Adurodija, H. Izumi, T. Ishihara, H. Yoshioka, H. Matsui, M. Motoyama, Appl. Phys. Lett. **74,** 3059 (1999).
[12] F. O. Adurodija, H. Izumi, T. Ishihara, H. Yoshioka, J. Vac. Sci. Technol. **A18**, 814 (2000).
[13] T. Aikainen, M. Ritala, W. M. Li, R. Lappalainen, M. Leskele, Appl. Surf. Sci. **112**, 231 (1997).
[14] A. Gurto, M. Ivanovskaya, A. Pfau, U. Weimer, W. Gopel, Thin Solid Films **307**, 288 (1997).
[15] H. Imai, A. Tominaga, H.Hirashima, M. Toki and N. Asakuma. J.Appl. Phys. **85**, 203(1999) .
[16] J. S. Cho, K. H. Yoon, S. K. Koh, J. Appl. Phys. **89,** 3223 (2001).
[17] A. H. M. Zahirul, P. K. Saha, T. Hata, K. Sasaki, Thin Solid Films **352**, 133 (1999).

[18] G. Golan, A. Axelevitch, E. Rabinovitch, J. Vac. Sci. Technol. **A16,** 2614 (1998).

[19] T. Minami, J. Vac. Sci. Technol. **A17,** 1765 (1999).

[20] B. Radhakrishna, T. K. Subramanyam, B. S. Naidu, S. Uthanna, Optical Mater. **15,** 217 (2000).

[21] M. Bender, N. Katsarakis, E. Gagaoudakis, E. Hourdekis, E. Douloufakis, V. Cimalla, G. Kiriakidis, J. Appl. Phys. **90,** 5382 (2001).

[22] Prathap, P. Gowridevi, G. Subbaiah, Y. P. V. Ramakrishna Reddy, K. T. Ganesan, V.: Curr. Appl. Phys. **8**, 120 (2008).

[23] Icdd Pdf-2 Data base, JCPDS-Int. Center for Diffraction Data, Pensylvania, 1994.

[24] Wang, C. Y. Cimalla, V. Romanus, H.Kups, T. Ecke, G. Stauden, T. Ali, M Lebedev, V. Pezoldt, J. Ambacher, O.: Appl. Phys. Lett. **89**, 011904 (2006).

[25] Wang, C. Y. Dai, Y. Pezoldt, J. Lu, B. Kups, T. Cimalla, V. Ambcher, O. : Cryst. Growth & Design **8**, 1257 (2008).

[26] Atou, T. Kusaba, K. Fukuoka, K. Kikuchi, M. Syono, Y. : J. Solid State Chem. **89**, 378 (1990).

[27] M. Kakimoto, M. Suzuki, T. Konishi, Y. Imai, M. Iwamoto and T. Hino,Chem.Lett., 5 (1986) 823.

[28] M.R. Shah, M.K. Alam, M.R. Karim and M.A. Sobhan, International Conference on Mechanical Engineering 2005 (ICME2005) 28- 30 December 2005, Dhaka, Bangladesh